Applied Catalysis B: Environmental 218 (2017) 679–689

Contents lists available at ScienceDirect

Applied Catalysis B: Environmental

journal homepage: www.elsevier.com/locate/apcatb

Nitrogen-doped mesoporous carbon supported Pt nanoparticles as a highly efficient catalyst for decarboxylation of saturated and unsaturated fatty acids to alkanes

Yingxin Liu[a], Xiaojie Yang[a], Haiyan Liu[b], Yuhua Ye[a], Zuojun Wei[b,*]

[a] Research and Development Base of Catalytic Hydrogenation, College of Pharmaceutical Science, Zhejiang University of Technology, Hangzhou 310014, PR China

[b] Key Laboratory of Biomass Chemical Engineering of the Ministry of Education, College of Chemical and Biological Engineering, Zhejiang University, Hangzhou 310027, PR China

ARTICLE INFO

Article history:
Received 14 February 2017
Received in revised form 29 May 2017
Accepted 21 June 2017
Available online 23 June 2017

Keywords:
Decarboxylation
Fatty acid
Fuel-range hydrocarbons
Nitrogen-doped mesoporous carbon
Pt catalyst

ABSTRACT

Mesoporous carbon (MC) and nitrogen-doped mesoporous carbon (NMC) were prepared through a dual-template approach with tetraethyl orthosilicate and Pluronic F127 as a dual-template, and phenol-formaldehyde and melamine-phenol-formaldehyde resins as carbon and carbon + nitrogen sources, respectively. Using them as the supports, the Pt/MC and Pt/NMC catalysts were prepared by incipient wetness impregnation method and used for the decarboxylation of saturated and unsaturated fatty acids to alkanes. Activated carbon supported Pt catalyst (Pt/AC) was also prepared for comparison. Among the three catalysts, Pt/NMC exhibited the highest catalytic performance, achieving yields of the corresponding alkanes of more than 97.0% from lauric, myristic, palmitic and stearic saturated acids and 44.0%–66.1% from oleic and linoleic unsaturated fatty acids. The turnover frequencies of Pt/NMC were estimated as 335–522 h^{-1} in the decarboxylation of saturated acids, which were almost 2-fold higher than Pt/MC and 3-fold higher than Pt/AC. The excellent performance of the Pt/NMC catalyst might be attributed to the introduction of N species to the MC support, which not only improved the anchoring and the dispersion of Pt nanoparticles on the catalyst surface, but also provided alkaline sites to adsorb carboxyl group in fatty acids.

1. Introduction

With the steady depletion of the fossil resources and the increasing demand for the liquid transportation fuels, renewable resources are more and more appealing as feedstocks for the production of fuels and chemicals. As an abundant and renewable resource, biomass has become the focus of numerous scientific and industrial research projects to produce biofuels as alternatives for fossil fuel. The use of lignocellulosic biomass or its derivatives to obtain high value-added products, such as 5-hydroxymethyl furfural and γ-valerolactone, to obtain biofuels such as 2,5-dimethyfuran from dehydration or deoxygenation processes [1–4], and to obtain "bio-oil" from hydrothermal deoxygenation process [5–8] has been extensively studied in the past thirty years. In the recent years, the fuel-range hydrocarbons derived from decarboxylation of fatty acids have been considered as the most promising alternatives owing to their excellent properties such as high energy density, low specific gravity and high storage stability [9–12].

In a decarboxylation process, oxygen atoms in fatty acids are removed as CO_2. It is therefore viewed as a competing method to other deoxygenation processes [13,14], as the latter requires a vital supply of H_2 to add to the carbonyl groups and remove oxygen atoms as H_2O, which increases the production costs and security risks. Catalytic deoxygenation of fatty acids in liquid phase by decarboxylation is performed preferably over activated carbon (AC) supported Pd or Pt catalysts. Fox example, Snåre et al. [15] studied the decarboxylation of stearic acid to *n*-heptadecane over kinds of heterogeneous catalysts with different combination of metals and supports, and found that Pd/AC and Pt/AC were the favorable catalysts for the reaction. Fu et al. [16] developed a hydrothermal deoxygenation approach to convert palmitic acid to *n*-pentadecane over Pt/AC, in which more than 90% of selectivity toward *n*-pentadecane was achieved.

Although AC is used as a classic catalyst support for the decarboxylation of fatty acids, there is a remarkable diffusion problem arisen from its microporous structure. To overcome the diffusion problem, larger porous supports such as γ-Al_2O_3 [13,17] and

* Corresponding author.
E-mail address: weizuojun@zju.edu.cn (Z. Wei).

http://dx.doi.org/10.1016/j.apcatb.2017.06.065
0926-3373/

zeolites [18–20] were more preferred. The newly developed mesoporous carbon (MC) with pore size distribution mainly between 3 and 12 nm [21,22] is a promising alternative catalyst support for the decarboxylation of fatty acids. Besides the better accessibility to the active sites of the substrates, MC takes the advantage of being easily modified with heteroatoms or functional groups to obtain desired physicochemical properties on its surface [23–26]. For example, MC treated by sulfonation possesses superior mesoporosity and high acidity, which endows excellent catalytic performance for esterification, dehydration, hydrolysis, and so on [26]. The modification of MC with nitrogen is generally viewed as an effective way to improve the size distribution and dispersion of the metals supported on it and increase the stability of the catalysts [27–30]. To the best of our knowledge, nitrogen-doped MC (NMC) materials have never been reported as the catalyst supports for decarboxylation reactions.

In the present work, MC and NMC were prepared through a dual-template approach. Using them as supports, Pt catalysts were prepared for the decarboxylation of four different saturated fatty acids, i.e. lauric, myristic, palmitic and stearic acids, and two unsaturated fatty acids, i.e. oleic and linoleic acids, which are prevalent in natural fatty esters and are always used as model substrates for the ultimate goal of decarboxylation of fatty acids and fatty esters [31–33]. For comparison, Pt catalyst supported on commercial AC was also prepared for the same reactions. Generally, when unsaturated C_{18} fatty acids (oleic and linoleic acid) are used as the reactants, molecular hydrogen or hydrogen transfer reagents is necessary for the addition of hydrogen to C=C double bonds presented in the molecules in order to achieve high selectivity to alkanes. Here, we investigated the decarboxylation of unsaturated fatty acids and saturated fatty acids in the absence of H_2 for the design of a sustainable process. The main purpose here is to investigate the role of nitrogen doping in the structure and the performance of NMC supported Pt catalyst for decarboxylation of fatty acids and develop highly efficient catalyst for decarboxylation of fatty acids to alkanes.

2. Experimental

2.1. Materials

$H_2PtCl_6{\cdot}6H_2O$ was purchased from Shanghai Jiuling Chemical Co. Ltd, China. Lauric acid, myristic acid, stearic acid, palmitic acid, oleic acid, linoleic acid, tetradecane and melamine were purchased from Aladdin Co. Ltd. Pluronic F127 ($EO_{106}PO_{70}EO_{106}$, Mw = 12600) was purchased from Sigma-Aldrich Co. Ltd. Other chemicals were purchased from Sinopharm Chemical Reagent Co. Ltd, China. All the chemicals used in this work were analytical reagents and were used without further purification.

2.2. Catalyst preparation

2.2.1. Preparation of NMC

A dual-templating approach [34,35] with minor modification was adopted to prepare NMC, in which tetraethyl orthosilicate and Pluronic F127 were used as hard and soft templates, respectively. The melamine-phenol-formaldehyde (MPF) resin was used as both the carbon and nitrogen precursors. The detailed preparation steps were as follows.

2.2.1.1. Preparation of MPF resin precursor. In a typical preparation, 20.0 g of phenol was melted at 40 °C in a 250 ml three-necked flask with reflux. Then 1.7 g of NaOH aqueous solution (20 wt%) was added slowly under stirring. After 10 min, 86.2 g of formalin (37 wt%) was added dropwisely, and the mixture was stirred for 30 min at 70 °C, followed by adding 17.8 g of melamine. The obtained milky solution was stirred at 70 °C for 4 h and cooled down to room temperature. After that its pH value was adjusted to about 7.0 by 2.0 M HCl and stood for stratification. The heavier phase was collected and diluted with ethanol to obtain 20 wt% MPF resin suspension.

2.2.1.2. Preparation of NMC. 15.6 g of tetraethyl orthosilicate (TEOS), 30.0 g of ethanol, and 7.5 g of 0.2 M HCl solution were added into a 250 ml flask under rigorous stirring, and pre-hydrolyzed at room temperature for 5 h to obtain solution A. 12.0 g of Pluronic F127 was dissolved in 60.0 g of ethanol to obtain a clarified solution B. Solution A, B and 37.5 g of the as-prepared MPF resin precursor suspension were mixed in a 250 ml flask under rigorous stirring at 70 °C for 2 h to obtain a homogeneous solution, and rotary evaporated to obtain a pale yellow gel. The gel was then treated with temperature-programmed calcination under Ar at 400 °C for 4 h, ramped to 800 °C with a heating rate of 20 °C min^{-1} and maintained for another 5 h to obtain N-doped mesoporous carbon-silica. Finally, the black mesoporous carbon-silica was alternatively treated with HF solution (20 wt%) to remove silica, followed by washing with double-distilled water until no fluoride, chloride and sodium ions were detectable. The remaining material was filtrated, dried under vacuum at 100 °C overnight, and denoted as NMC.

For comparison, mesoporous carbon (MC) without N was prepared through the same procedure only without using melamine.

2.2.2. Preparation of Pt catalysts

NMC supported Pt catalyst was prepared by an incipient wetness impregnation method. 0.04 mmol of $H_2PtCl_6{\cdot}6H_2O$ (corresponding to 3 wt% of theoretical Pt loading in the final catalyst) was dissolved in 1 ml of double-distilled water and then slowly added to 0.5 g of NMC support at room temperature. After impregnated for 24 h, the mixture was dried under vacuum at 110 °C for 10 h and finally reduced at 350 °C in a tubular furnace under hydrogen flow for 4 h to obtain the target catalyst, which was denoted as Pt/NMC.

For comparison, MC and AC supported Pt catalysts were also prepared by using the same method, and denoted as Pt/MC and Pt/AC, respectively. The Pt loading in the three catalysts was 3 wt%.

The preparation processes for the Pt/NMC catalyst are illustrated in Scheme 1.

2.3. Catalyst characterization

X-ray powder diffraction (XRD) patterns were recorded with an XRD-600 diffractometer (Shimadzu Co., Japan) using a Cu Kα radiation (λ = 0.15406 nm) in a Bragg-Brentano parafocusing optics configuration (40 kV, 40 mA). Samples were scanned from 10 to 80° with a scanning rate of 4° min^{-1} and a step size of 0.02°. The crystalline phases were identified by reference to the JCPDS database.

Transmission electron microscopy (TEM) and high-angle annular dark-field scanning TEM (HAADF-STEM) images were obtained using a Tecnai G2 F30 S-Twin instrument (FEI Co., USA) operated at an accelerating voltage of 300 kV. Samples were prepared by dispersing the catalyst powder in ethanol under ultrasound for 15–20 min and then dropping the suspension onto a copper grid coated with carbon film. Particle size distribution of Pt nanoparticles in each sample was determined from the corresponding TEM image by measuring the sizes of more than 200 particles.

BET specific surface areas and pore structures were measured by pulsed nitrogen adsorption-desorption method at −196 °C using an ASAP 2010 instrument (Micromeritics Instrument Co.). Prior to N_2 physisorption, the samples were degassed under vacuum at 250 °C overnight. The specific surface area was calculated by using the Brunauer-Emmett-Teller (BET) method, and the pore size distribution and pore volume were measured by using Barrett-Joyner-Halenda (BJH) analysis from the adsorption branch of the isotherms.

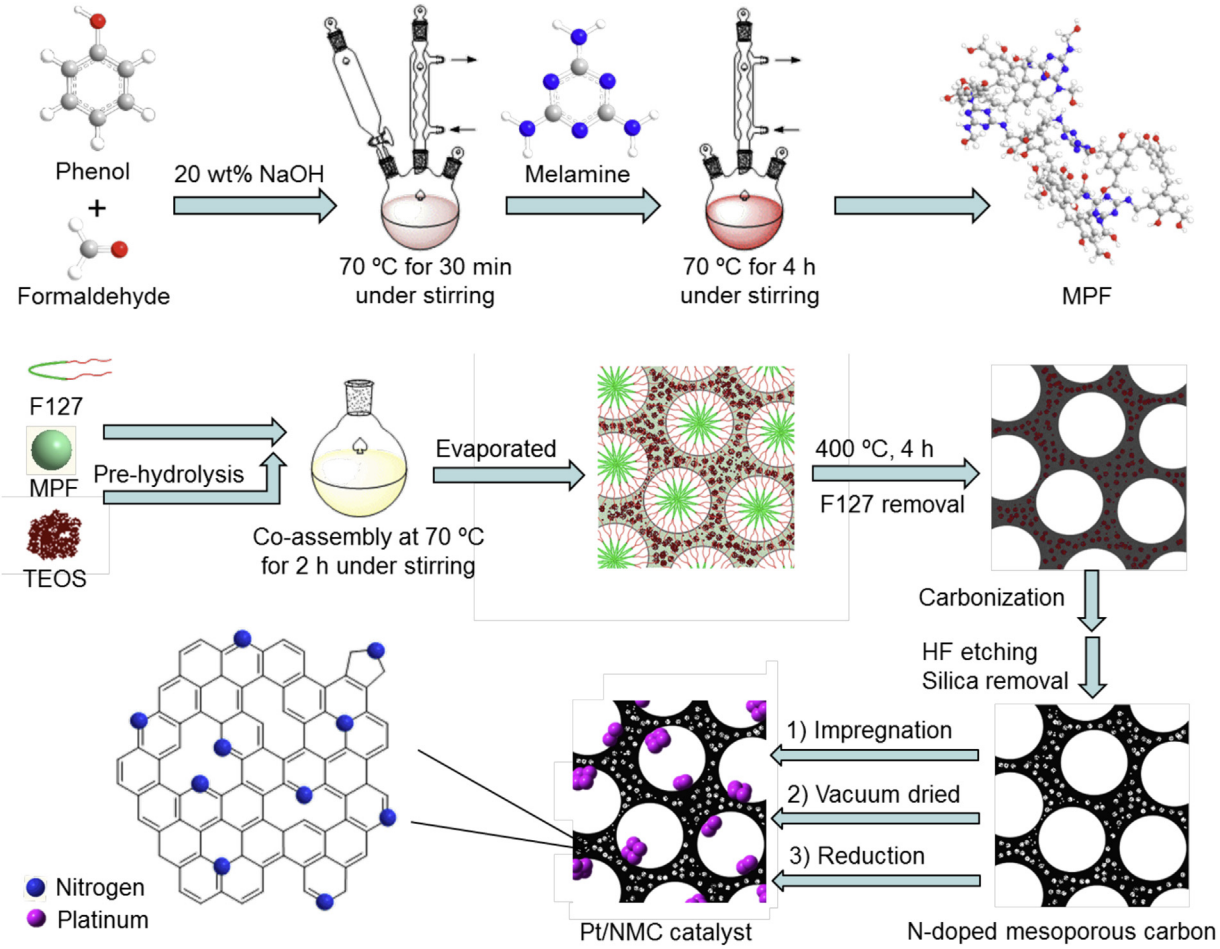

Scheme 1. Preparation processes for Pt/NMC catalyst.

The metal dispersion and particle size were measured by CO-chemisorption at 35 °C using a Micromeritics ASAP 2020 system. Prior to adsorption measurement, an amount of sample was evacuated at 120 °C for 30 min, heated to 350 °C at a ramp rate of 10 °C min^{-1} in pure hydrogen and reduced at this temperature for 4 h, followed by evacuating at 370 °C for 3 h, cooling to 35 °C and further evacuating at 35 °C for 30 min. Subsequently, CO chemisorption measurements were carried out via the double isotherm method.

The alkalinity of the catalysts was measured by temperature programmed desorption of CO_2 (CO_2-TPD). Prior to the measurement, the sample was reduced at 350 °C in H_2 flow for 4 h and cooled to room temperature. Then the sample was saturated with pure CO_2 (50 ml min^{-1}) for 30 min, and flushed with N_2 flow to remove all physically adsorbed molecules. After that, the TPD experiment was started with a heating rate of 10 °C min^{-1} from room temperature to 600 °C under N_2 flow (50 ml min^{-1}). The desorbed CO_2 was monitored on-line by an Extrel mass spectrometer.

X-ray photoelectron spectroscopy (XPS) spectra were obtained using an Escalab Mark II X-ray spectrometer (VG Co., United Kingdom) equipped with a magnesium anode (Mg Kα = 1253.6 eV). Energy corrections were performed using a 1s peak of the pollutant carbon at 284.6 eV. The sample was prepared by pressing the catalyst powder onto the surface with silver sol gel.

The N content in NMC supports was determined by using a LECO-CHNS932 elemental analysis (EA) instrument (LECO Co., United States). The contents of H, N and C were directly measured by the instrument, while the content of O was calculated by assuming the material contained only the four elements [36].

Pt content in the reaction solution was determined using a Varian AA 240 FS atomic adsorption spectrophotometer (AAS; Varian, Inc., USA).

2.4. Reaction procedure

Decarboxylation reactions of fatty acids were conducted in 1.67 ml unstirred mini-batch reactors assembled from 3/8-inch stainless steel Swagelok parts, similar to ref [37,38]. Prior to being used, the reactor was rinsed with acetone, followed by washing with water at 300 °C for 30 min to remove any residual materials. In a typical experiment, 15 mg of catalyst together with 50 mg of fatty acid and 1 ml of solvent tetradecane was added into the reactor. Then the reactor was sealed and immersed into a sand bath with desired temperature to initiate the reaction. After the reaction was done, the reactor was taken out from the sand bath, cooled down in a water bath to room temperature immediately, and sampled for analysis. No H_2 was added to the reactors in any of these experiments.

The reaction products were analyzed by using an Agilent 7890 gas chromatograph equipped with a HP-5 capillary column (30.0 m × 0.32 mm × 0.25 μm) and a flame ionization detector (FID). The column temperature was raised from 70 to 280 °C with a ramp of 10 °C min^{-1}. The temperatures of the injector port and the detector were 280 °C and 300 °C, respectively. Naphthaline was used as an interior standard for accurate quantification of lauric, myristic, palmitic, stearic, oleic and linoleic acids, and hydrocarbons of octadecane, heptadecane, tetradecane, dodecane, and hexane. The correction factors to naphthaline were detected as

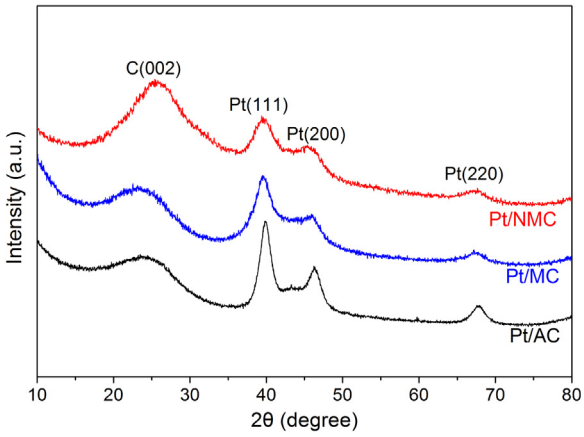

Fig. 1. Wide-angel XRD patterns of Pt/NMC, Pt/MC and Pt/AC catalysts.

0.99, 0.96, 0.97, 0.99, 0.98, 0.98, 1.02, 1.03, 1.05, 1.00, and 1.03, respectively.

Product identification was performed with an Agilent 6890 gas chromatography system coupled to a mass spectrometer equipped with an Agilent 5973 quadrupole mass analyzer. The chromatographic analysis was conducted with an injector temperature of 280 °C and a HP-5 capillary column (30.0 m × 0.25 mm × 0.32 μm) with helium flow of 2.0 ml min^{-1} and a 1:10 split ratio. The oven was heated using the following temperature program: initial temperature of 100 °C increased to 280 °C at a ramp of 12 °C·min^{-1} and maintained for 10 min. The mass spectrometer was operated in electron ionization (EI) mode at an energy of 70 eV.

3. Results and discussion

3.1. Characterization of the catalysts

Fig. 1 shows the wide-angle XRD patterns of the as-prepared Pt/NMC, Pt/MC and Pt/AC catalysts. It can be seen that the curves for all the three catalysts exhibit a broad diffraction peak at around 25°, which corresponds to (002) diffraction from graphitic carbon [39–41]. The relative intensity of carbon (002) peak for Pt/NMC is obviously higher than those for Pt/MC and Pt/AC, indicating that a better graphitic network structure is formed in the presence of nitrogen [42]. Moreover, the diffraction peak of carbon (002) in Pt/NMC sample displays a slight positive shift (from 24° to 25.3°) compared with those in Pt/MC and Pt/AC samples, indicating that the doped-nitrogen atoms may cause the framework shrinkage, destroy the lattice of graphite crystal, and finally lead to the decrease in d-spacing of the (002) crystal plane in the graphitic structure [43,44]. In all the three samples, the (111), (200) and (220) diffraction peaks of Pt at 2θ values of around 39.8°, 46.2° and 67.8° are observed, revealing the presence of crystalline platinum metal Pt(0) with face centered cubic (fcc) lattice (JCPDS No. 65–2868) [45,46]. The average sizes of Pt nanoparticles calculated from the Pt (111) peaks by using the Scherrer's formula $D = k\lambda/\beta\cos\theta$ were 2.0, 3.5 and 5.0 nm for Pt/NMC, Pt/MC and Pt/AC, respectively (Table 1).

The morphology and the sizes of Pt nanoparticles on Pt/NMC, Pt/MC and Pt/AC catalysts were characterized by TEM (Fig. 2). The inset in Fig. 2(a) displays a typical lattice fringe with a spacing of 0.23 nm, which corresponds to the (111) plane of Pt [47–50], indicating the observation of Pt nanoparticles. The size distribution of Pt nanoparticles on each sample (insets in Fig. 2(a), (f) and (g)) is determined from the corresponding TEM images by measuring the size of more than 200 randomly selected Pt nanoparticles. As expected, Pt nanoparticles on NMC display fairly smaller size and narrower size distribution of 2.2 ± 1.2 nm, which was further confirmed by HAADF-STEM image as shown in Fig. 2(b). The TEM images for the Pt/MC and Pt/AC catalysts, however, display larger sizes and broader size distributions of 3.1 ± 1.6 nm and 4.7 ± 1.6 nm, respectively (Fig. 2(f) and (g)), which are in good agreement with the aforementioned XRD results (Table 1). Moreover, as evidenced by the 2D atomic mapping (Fig. 2(e)), the nitrogen atoms are homogeneously distributed throughout the whole area of the porous carbon [51,52]. All these results indicate that nitrogen doping contributes to the nucleation and growth kinetics of Pt nanoparticles, leading to the formation of smaller particles with uniform dispersion [46,48,53].

Fig. 3 displays the nitrogen sorption isotherms for the supports and the Pt catalysts, and the corresponding structural parameters are listed in Table 1. It can be seen from Fig. 3(a) that both NMC and MC, including the corresponding supported Pt catalysts (Pt/NMC and Pt/MC), exhibit type IV isotherms with H1 hysteresis loops at the higher relative pressure of 0.4–0.9, typically associated with the mesoporous structure feature [54,55]. In contrast, Pt/AC shows typical type I isotherm without hysteresis loop, indicating that Pt/AC mainly consists of micropores. Both NMC and MC have considerable high BET specific surface areas of more than 1000 m^2 g^{-1}, which is in agreement with the previous reports [56,57]. Compared with MC, NMC displays lower BET specific surface area (1152 m^2 g^{-1} vs. 1473 m^2 g^{-1}), smaller average mesopore size (4.3 nm vs. 4.7 nm) and lower total pore volume (1.15 cm^3 g^{-1} vs. 2.24 cm^3 g^{-1}) (Table 1). This is probably due to the introduction of nitrogen atoms which makes the mesoporous channels be transformed or even collapsed [43]. Moreover, after loading Pt, the BET specific surface area, average mesopore size and total pore volume of Pt/NMC decrease more remarkablly than those of Pt/MC, indicating that the more conducive occupation of Pt nanoparticles on the N-doped mesoporous pores and certain block of NMC channels (Table 1) [58,59].

The dispersion of Pt nanoparticles on the catalyst surface was further determined by CO chemisorptions and the results are presented in Table 1, which are 61.3%, 42.5%, and 30.1% for Pt/NMC, Pt/MC and Pt/AC, respectively. The dispersion of Pt nanoparticles on the Pt/NMC catalyst is remarkably higher than those on the Pt/MC and Pt/AC catalysts, suggesting that nitrogen doping can increase the dispersion of Pt nanoparticles on the Pt/NMC catalyst surface, in good agreement with the above XRD results. From Table 1 we can see that the values of the Pt dispersion obtained from CO chemisorption are about 16–20% larger than the data estimated from the average particle sizes calculated by Scherrer formula. This is reasonable, as a quantity of Pt nanoparticles with diameters far less than average size were also contributable to CO adsorption and could serve as active sites during the decarboxylation reaction [59].

XPS measurement was conducted to analyze the element composition and their electronic states on the catalyst surface. The full scan spectra of Pt/MC and Pt/NMC (Fig. 1 s and Fig. 2s) show no obvious peak of Na, Cl and F element, indicating these elements were fully removed from the carbon bulk during the washing process. As shown in Fig. 4(a), the wide scan spectra reveal the presence of C and O with strong peaks at around 285 eV (C1s) and 532 eV (O1s) in the three Pt catalysts used in this work. The peak corresponding to Si element is not observed in the Pt/MC and Pt/NMC catalysts, which means that the silica was fully removed by our treatment with HF during the catalyst preparation [59]. The peak at around 400 eV assigned to N 1s is found in the Pt/NMC catalyst, indicating the successful doping of nitrogen [60]. To get a more precise description of the chemical identity of surface nitrogen atoms on the Pt/NMC catalyst, the binding energies of C 1s and N 1s were re-scanned at high resolution and the corresponding peaks were fitted with Voigt functions. As shown in Fig. 4(b), the XPS spectrum of N 1s exhibits four peaks with the binding energies centered at about 398.2, 400.0, 400.8 and 402.7 eV, assigned to pyridinic-N (N-6), pyrrolic-N (N-5),

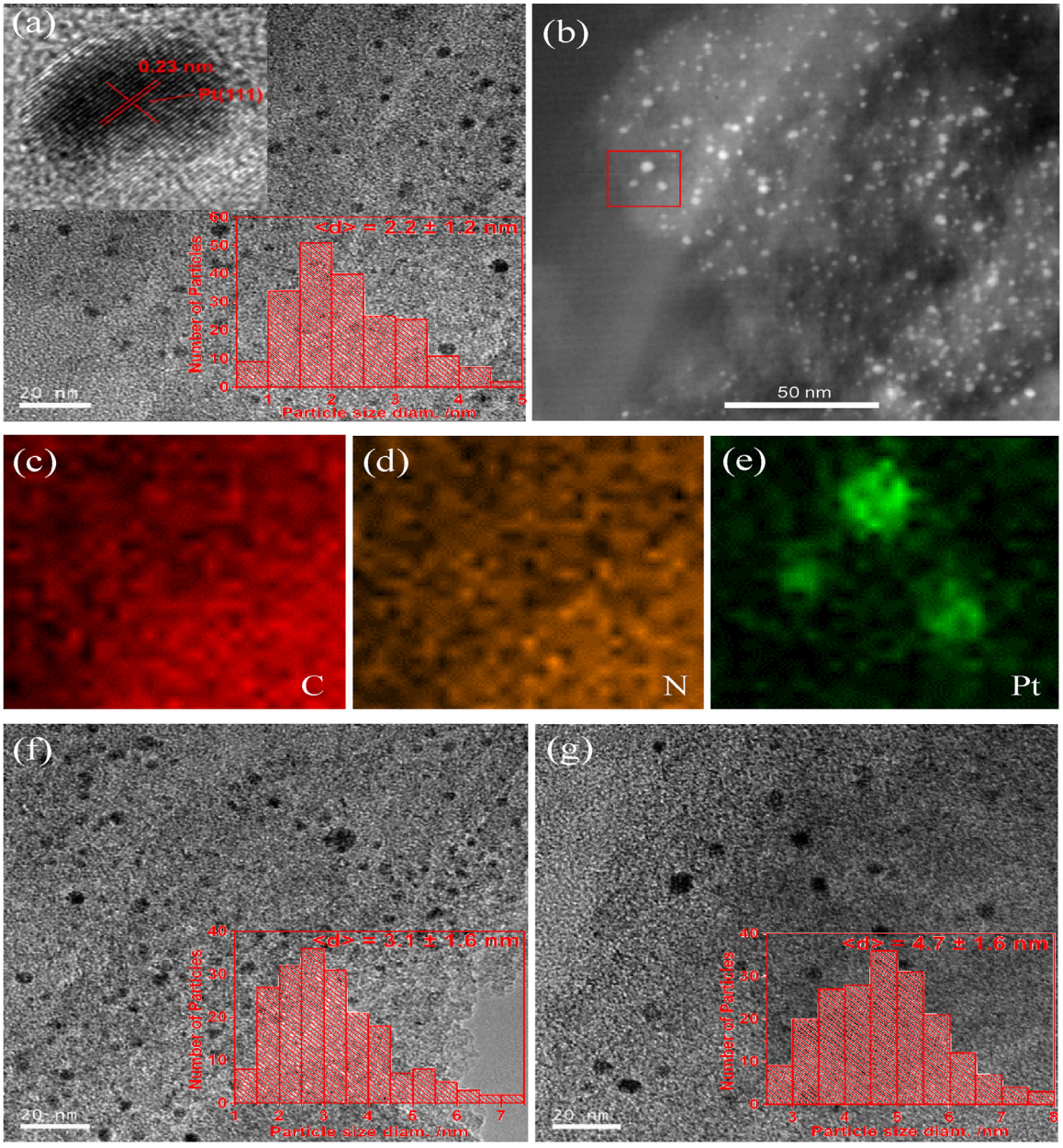

Fig. 2. TEM images of Pt catalysts. (a–e) TEM and HAADF-STEM images of Pt/NMC catalyst with corresponding elemental mappings (a color version of this figure can be viewed online). (f) and (g) TEM images of Pt/MC and Pt/AC. The insets are the regular lattice image and the size distributions of Pt nanoparticles.

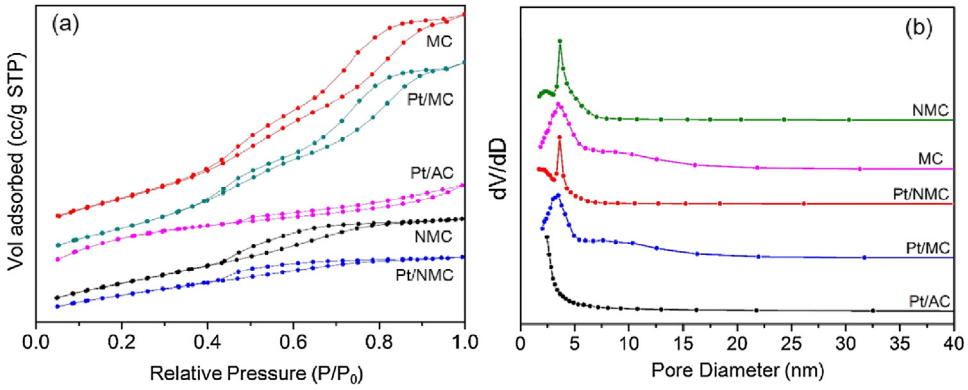

Fig. 3. Nitrogen sorption isotherms (a) and the corresponding pore size distribution curves (b) of the samples.

Table 1
Textural properties of various samples and size and dispersion of Pt nanoparticles.

Sample	$d_{Pt(111)}$[a] (nm)	d_{TEM} (nm)	Dispersion of Pt (%)		S_{BET} ($m^2\ g^{-1}$)	D_{BJH} (nm)	V_{tot} ($cm^3\ g^{-1}$)
			Predicted[b]	Determined[c]			
NMC	–	–	–	–	1152	4.3	1.15
MC	–	–	–	–	1473	4.7	2.24
Pt/NMC	2.0	2.2 ± 1.2	51.4	61.3	904	3.1	0.73
Pt/MC	3.5	3.1 ± 1.6	36.5	42.5	1416	4.6	2.05
Pt/AC	5.0	4.7 ± 1.6	24.0	30.1	1627	2.9	1.20

[a] Estimated by the Scherrer formula $D = k\lambda/\beta\cos\theta$ based on Pt (111) peaks.
[b] Predicted by the formula $D = M_{Pt} \times 6 \times \rho_{site}/(\rho_{metal} \times N \times d)$, where $M_{Pt} = 195.1\ g\ mol^1$, $\rho_{metal} = 21.45\ g\ cm^3$, $\rho_{site} = 12.5$, and d (nm) is the average Pt particle size obtained according to XRD results.
[c] Determined by CO chemisorption.

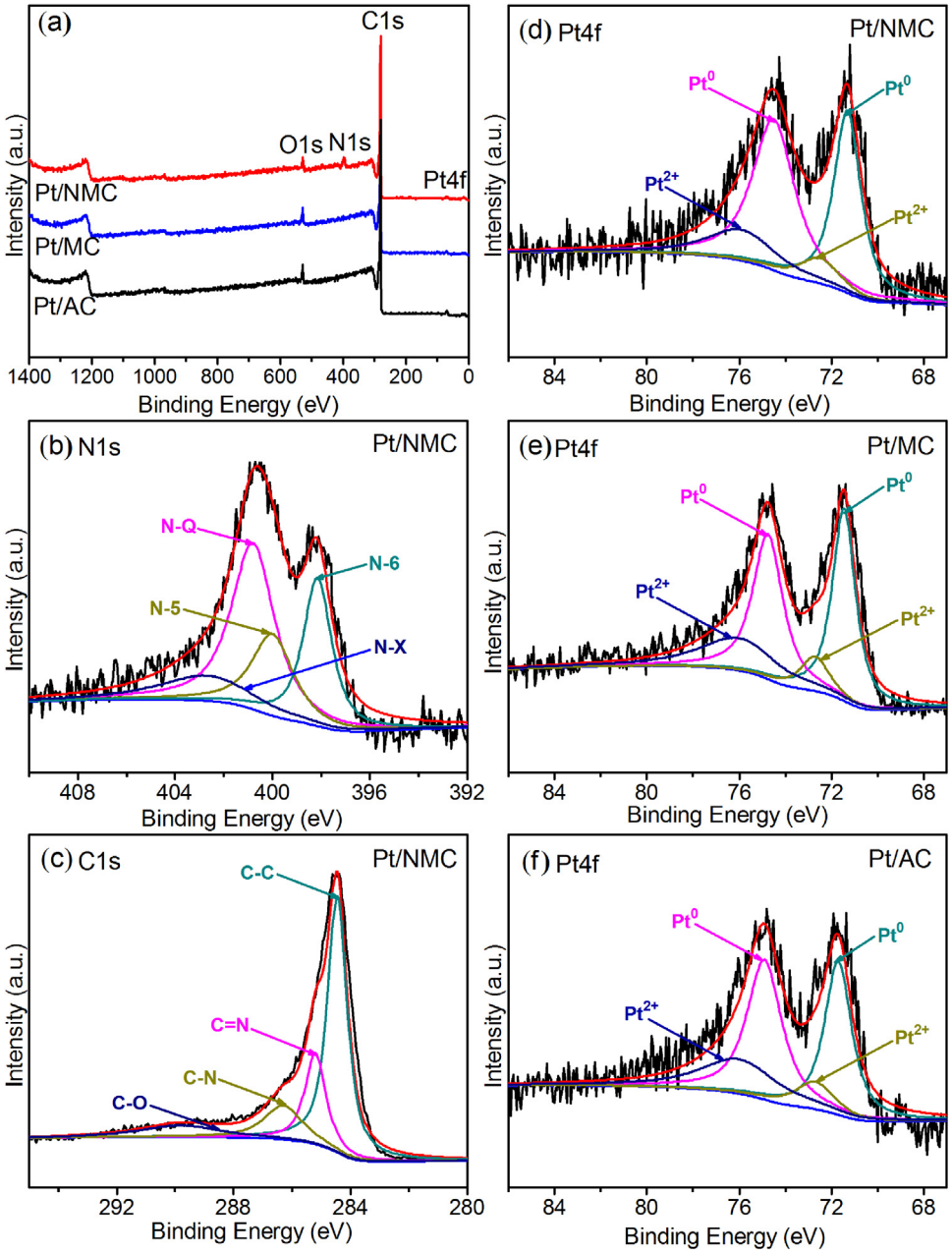

Fig. 4. (a) XPS survey spectra of the samples; (b–d) N1s, C1s and Pt 4f XPS spectra of Pt/NMC; (e) and (f) Pt 4f XPS spectra of Pt/MC and Pt/AC.

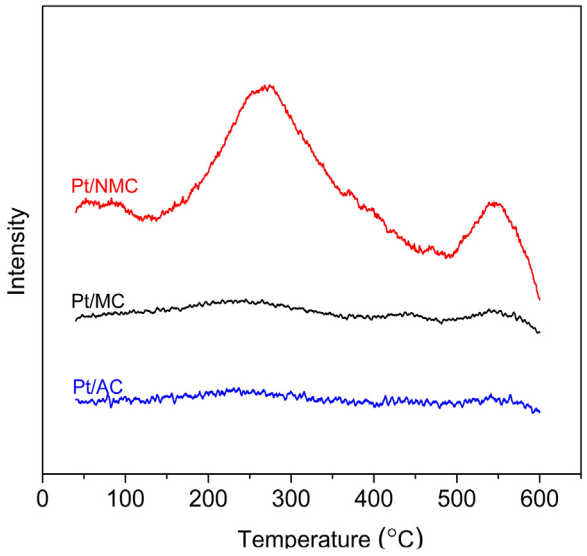

Fig. 5. CO_2-TPD profiles of Pt/NMC, Pt/MC and Pt/AC catalysts.

graphitic-N (N-Q) and pyridinic nitrogen-oxide (N-X), respectively [42,43,60,61]. It has been reported that N-5 and N-6 may provide the main initial nucleation sites for the deposition of Pt [62], preventing Pt particles from sintering and improving Pt particles being anchored strongly on the NMC support [63]. As in our case, the peaks of N-5 and N-6 dominate nearly 50 atom% of the full signal, which may contribute to the homogenous dispersion of Pt nanoparticles on the NMC support observed in the above XRD, TEM and CO chemisorptions results. Fig. 4(c) shows the high-resolution C 1s spectrum of the Pt/NMC catalyst, with four components peaked at 284.5, 285.2, 286.3 and 289.8 eV, corresponding to the C—C, C═N, C—N and C—O bonds, respectively [50,54,61]. The FT-IR spectrum of NMC also showed the C═N stretching and N—H stretching vibrations (Fig. 3s). These results further suggest that the nitrogen atoms are effectively incorporated into the carbon frameworks.

The Pt 4f spectra of Pt/NMC, Pt/MC and Pt/AC are displayed in Fig. 4(d), (e) and (f), respectively. The relative quantitative analysis was measured by the integrated intensities of the deconvoluted XPS signals and the results are shown in Table 2. It can be seen that each Pt 4f spectrum of the three Pt catalysts could be deconvoluted into two pairs of doublets. The more intense doublet (the peak at 71.2 ~ 71.5 eV and the peak at 74.4 ~ 74.7 eV) is assigned to Pt $4f_{7/2}$ and Pt $4f_{5/2}$ excitations of metallic Pt(0), whereas the less intense doublet (the peak at 72.4 ~ 72.6 eV and the peak at 75.7 ~ 76.0 eV) is ascribed to Pt(II). Compared with Pt/MC and Pt/AC, an obvious negative shift (ca −0.3 eV) of Pt 4f peaks can be observed in the XPS spectrum of Pt/NMC. This shift was also observed by other researchers, which was generally attributed to a strong interaction between nitrogen groups and Pt nanoparticles, leading to electron transfer in Pt/NMC from NMC to Pt, and increasing the reduction probability of Pt ions in the end [50,54,61]. No apparent shift is found in the Pt 4f spectrum of Pt/AC in comparison with that of Pt/MC (Table 2). This could be contributed to the similar oxygen contents in the two catalysts, which donates similar intensity of electrons to Pt [35]. The surface element scanning data show that Pt content on the Pt/NMC catalyst surface is 1.19 wt%, which is lower than those on Pt/MC and Pt/AC, and also lower than the bulk content (~3.0 wt%), suggesting that Pt particles tend to be embedded into the pores of the NMC materials [64].

The basic density and strength properties of Pt/NMC, Pt/MC and Pt/AC were determined by CO_2-TPD. As shown in Fig. 5, both Pt/AC and Pt/MC show very low or almost no CO_2 absorption peaks, suggesting that the basic sites in these two catalysts are very scarce.

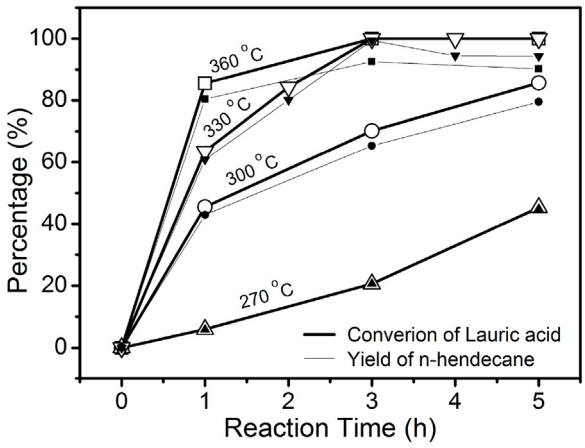

Fig. 6. Reaction kinetics for decarboxylation of lauric acid over Pt/NMC catalyst. Reaction conditions: catalyst, 15 mg; lauric acid, 50 mg; tetradecane, 1 ml.

It is worth noting that the Pt/NMC catalyst exhibits two peaks at 228 and 550 °C, which is consistent with the results reported by Abdulkareem-Alsultan [65] and Xu [66]. The concentration of base cites of NMC was estimated as ca 132 μmol CO_2 per gram NMC. The peaks may be contributed to the basic sites associated with the weak chemical and physical adsorption of CO_2. As discussed in the above XPS characterization, these basic sites origin from the N-containing groups, such as CN heterocycles and the pyridinic nitrogen-oxide at the edge of the graphitic sheets. Combined with the following results of the decarboxylation of fatty acids, it is suggested that the basic sites in the Pt/NMC catalyst may accelerate the adsorption of acidic substrate to the vicinity of metal particles and therefore improve the decarboxylation reaction [3].

3.2. Decarboxylation of fatty acids

3.2.1. Reaction optimization

Firstly, lauric acid was used as the substrate to optimize the decarboxylation reaction conditions, including reaction temperature and time over NMC (carbonized at 800 °C) supported Pt catalyst. Fig. 6 presents the reaction kinetics for decarboxylation of lauric acid from 270 °C to 360 °C. It can be seen from Fig. 6 that both the conversion of lauric acid and the yield of target product *n*-hendecane increased singularly with the increase in reaction temperature from 270 to 330 °C, and peaked at 330 °C with the highest *n*-hendecane yield of 99.4%. At higher temperature of 360 °C, the conversion of lauric acid maintained 100% while the selectivity to *n*-hendecane decreased to 92.6%, suggesting the thermal cracking of *n*-hendecane into lower alkane fractions at this temperature [38]. With the increase in reaction time, the conversion of lauric acid and the yield of *n*-hendecane increased and reached flat at 3 h, with 100% conversion of lauric acid and 99.4% yield of *n*-hendecane. We therefore determined 330 °C and 3 h as the optimal reaction temperature and time for the following reactions.

The effect of carbonization temperature of the NMC support on the property of the >Pt/NMC catalyst was further investigated and the results are listed in Table 3. It can be seen that when the carbonization temperature of NMC increased from 600 to 1000 °C, the nitrogen contents of the corresponding Pt/NMC catalysts decreased from 12.3 to 3.1 wt%, indicating the removal of nitrogen at elevated temperatures [42,67]. However, the catalytic performance of the Pt/NMC catalysts for the decarboxylation of lauric acid seemed independent on the nitrogen, since the Pt catalyst supported on the NMC carbonized at 800 °C which has middle nitrogen content achieved the highest yield of *n*-hendecane (99.4% with 100% con-

Table 2
XPS relative quantitative analysis and element analysis.

Catalyst	Surface Pt (0)		Surface Pt (II)		Surface element (at%)		
	B.E.[a] $4f_{7/2}/4f_{5/2}$ (eV)	Area (%)	B.E. $4f_{7/2}/4f_{5/2}$ (eV)	Area (%)	Pt	O	N
Pt/NMC	71.2/74.4	79.6	72.4/75.7	20.4	1.19	5.90	6.20
Pt/MC	71.5/74.7	74.4	72.6/76.0	25.6	1.80	5.99	0
Pt/AC	71.5/74.7	75.2	72.5/75.9	24.8	2.19	6.61	0

[a] Abbreviation of binding energy.

Table 3
Effect of carbonization temperature of NMC on the performance of Pt/NMC catalyst for decarboxylation of lauric acid.

NMC carbonization temp. (°C)	S_{BET} ($m^2\ g^{-1}$)	N (wt%)[a]	Dispersion of Pt (%)[b]	Conversion (%)	n-Hendecane yield (%)
600	666	12.3	44.3	69.1	66.4
800	1152	8.6	61.3	100	99.4
1000	1008	3.1	58.5	91.7	91.2

Reaction conditions: catalyst, 15 mg; lauric acid, 50 mg; tetradecane, 1 ml; T, 330 °C; reaction time, 3 h.
[a] Detected by elemental analysis.
[b] Determined by CO chemisorption.

version of lauric acid). The poor yield of *n*-hendecane obtained over the Pt catalyst supported on the NMC carbonized at 600 °C is usually ascribed to the incomplete carbonization of the carbon material, which decreases its specific surface area (only 666 $m^2\ g^{-1}$, Fig. 4s) and also the Pt dispersion (44.3%) [68]. The Pt catalyst supported on the NMC carbonized at 1000 °C achieved slight low yield of *n*-hendecane compared with the sample supported on the NMC carbonized at 800 °C, probably due to the too low content of N (3.1%), which decreased the interaction between the substrate and the support. Moreover, higher carbonization temperature at 1000 °C may also change the pyridinic-N (N-6) and pyrrolic-N (N-5) to other forms of nitrogen dopants, resulting in negative effects on Pt dispersion and the catalytic performance as discussed above [52,54]. We therefore chose the Pt catalyst supported on the NMC carbonized at 800 °C for the following research.

3.2.2. Decarboxylation of saturated fatty acids

The catalytic performance of the as-prepared Pt/NMC, Pt/MC and Pt/AC catalysts was tested for the decarboxylation of several saturated fatty acids, including lauric, myristic, palmitic and stearic acids (Table 4). As expected, Pt/NMC exhibited the best performance for the decarboxylation of all the four saturated fatty acids used in this work, over which the conversion of each fatty acid reached 100% and the yields of the corresponding alkanes were more than 97% (entries 1, 5, 8 and 11). The catalytic performance of Pt/MC ranked the second, giving moderate conversions (<88.2%) and alkanes yields (60–83%) (entries 2, 6, 9 and 12). Pt/AC showed the poorest performance at the same reaction conditions (entries 3, 7, 10 and 13). These results suggest that N-doping is beneficial to improving the activity of the Pt-based catalysts, which was further demonstrated by the estimation of the initial reaction rates. As shown in Table 4, the turnover frequencies (TOFs) of Pt/NMC estimated at 10 min for each substrate (335–522 h^{-1}) were almost 2-fold higher than Pt/MC (179–289 h^{-1}) and 3-fold higher than Pt/AC (112–162 h^{-1}). Additionally, it should be noted that since decarboxylation reaction in our work was conducted for 3 h, this is why we obtained obvious lower conversions and yields over Pt/AC than those ever reported [15,37]. Actually, when the reaction time was prolonged to 5 h, a considerable high yield of *n*-hendecane was achieved over Pt/AC (91.2%, entry 4). The decarboxylation of lauric acid with bare NMC, NM or AC as catalyst was also conducted for comparison (entries 5–7). The results showed that the conversion of lauric acid fell in the range of 40.6%-45.5%, with slight change over different carbon materials. The *n*-hendecane yields were exclusively less than 1%, indicating Pt takes the mail role for decarboxylation of fatty acids.

3.2.3. Decarboxylation of unsaturated fatty acids

The performance of Pt/NMC for the decarboxylation of unsaturated fatty acids was also tested. Generally, the decarboxylation of unsaturated fatty acids was conducted with hydrogen or other hydrogen sources, as the hydrogenation of the C=C bond plays an important role in the following decarboxylation reaction. Here, four hydrogen sources, i.e. methanol, water, glycerol and isopropanol, were used as the hydrogen sources for the decarboxylation of oleic acid over Pt/NMC. As shown in Table 5, when using isopropanol as the hydrogen source, the highest *n*-heptadecane yield achieved (66.1%, entry 21), followed by methanol (58.9%, entry 18), water (23.1%, entry 19) and glycerol (16.4%, entry 20). It seemed that water and glycerol were not effective for *n*-heptadecane production in our work, since in these two cases comparable or even lower *n*-heptadecane yields were obtained compared with the case without adding any hydrogen source (19.9%, entry 17). For comparison, the decarboxylation of oleic acid was also studied over Pt/MC and Pt/AC using isopropanol as the hydrogen source (entries 22 and 23), obtaining *n*-heptadecane yields of only 35.6% and 30.3%, respectively. When linoleic acid, having one more C=C bond than oleic acid, was applied as the substrate, the catalytic performance of Pt/NMC, Pt/MC and Pt/AC decreased. However, Pt/NMC still exhibited the highest performance, followed by Pt/MC and Pt/AC (entry 24, 25 and 26).

3.2.4. Recyclability of Pt/NMC catalyst

The recyclability of Pt/NMC for the decarboxylation of lauric acid was investigated. After reaction, Pt/NMC was centrifugated, washed with tetradecane, and returned to the reactor for reuse. As shown in Fig. 7(a), the Pt/NMC catalyst exhibited a good recyclability for the decarboxylation of lauric acid. It could be reused at least three times with only approximate 9.4% of decrease in *n*-heptadecane yield. A part of the reasons for the decrease in the activity of the reused catalyst may be ascribed to the loss during post processing due to it's a very small amount (only 15 mg). In another recyclability test, we scaled up the catalyst amount to 50 mg in the same reactor (only the 1.67-ml mini reactors from Swagelok was available in our lab that can operate at as high as 300 °C) trying to remove the effect of catalyst loss during cycles. As shown in Fig. 7(b), the stability of Pt/NMC was greatly improved: the conversion of lauric acid dropped from 99.5% down to 90.4%, and the yield of *n*-hendecane dropped slightly from 99.5% to 95.7% after eight cycles. TEM analysis of the eight-reused Pt/NMC showed

Table 4
Decarboxylation of saturated fatty acids over Pt-based catalysts.

Entry	Catalyst	Substrate	Decarboxylation product	Conversion(%)	Yield(%)	TOF(h^{-1})
1	Pt/NMC	Lauric acid	n-Hendecane	100	99.4	622
2	Pt/MC			88.2	82.8	337
3	Pt/AC			72.8	67.5	203
4	Pt/AC[a]			98.7	91.2	–
5	NMC			45.5	<1	–
6	MC			43.1	<1	–
7	AC			40.6	<1	–
8	Pt/NMC	Myristic acid	n-Tridecane	100	99.1	400
9	Pt/MC			79.6	60.5	209
10	Pt/AC			45.2	35.4	142
11	Pt/NMC	Palmitic acid	n-Pentadecane	100	98.5	406
12	Pt/MC			81.4	74.1	230
13	Pt/AC			78.3	73.7	141
14	Pt/NMC	Stearic acid	n-heptadecane	100	97.2	469
15	Pt/MC			83.1	71.8	283
16	Pt/AC			50.3	54.2	176

Reaction conditions: catalyst, 15 mg; FA, 50 mg; tetradecane, 1 ml; T, 330 °C; reaction for 3 h. TOF was estimated based on the conversions of fatty acids at 10 min of reaction and surface Pt determined by CO chemisorption.
[a] Reaction time is prolonged to 5 h.

Table 5
Decarboxylation of unsaturated fatty acids over Pt-based catalysts.

Entry	Catalysts	Substrate	Hydrogen source	Conversion (%)	n-Heptadecane yield (%)
17	Pt/NMC	Oleic acid	–	99.5	19.9
18	Pt/NMC	Oleic acid	Methanol	95.4	58.9
19	Pt/NMC	Oleic acid	Water	80.3	23.1
20	Pt/NMC	Oleic acid	Glycerol	78.2	16.4
21	Pt/NMC	Oleic acid	Isopropanol	92.0	66.1
22	Pt/MC	Oleic acid	Isopropanol	82.1	35.6
23	Pt/AC	Oleic acid	Isopropanol	96.3	30.3
24	Pt/NMC	Linoleic acid	Isopropanol	87.0	44.0
25	Pt/MC	Linoleic acid	Isopropanol	77.5	30.4
26	Pt/AC	Linoleic acid	Isopropanol	70.2	11.1

Reaction conditions: catalyst, 15 mg; FA, 50 mg; tetradecane, 1 ml; mole ratio of hydrogen donor to FA, 10:1; T, 330 °C; reaction for 3 h.

that aggregation of Pt particles with diameter larger than 5 nm was formed (Fig. 8). We further detected the Pt concentration in the reaction bulk to check the leakage of Pt: in each cycle solution, the Pt concentration is ca 50 mg l^{-1} (Fig. 8), corresponding to 0.1 w% of Pt in the bulk Pt/NMC catalyst.

The stability of the doped nitrogen would impact heavily on the catalytic performance of Pt/NMC. We therefore carefully determined the nitrogen content in the spent catalyst (after eight cycles) by three times: the averaged value of the nitrogen content is (8.3 ± 0.2) wt%, which decreased ca 3.5% comparing to that in the fresh catalyst (8.6 wt%). We therefore consider that the aggregation of Pt particles and the leakage of Pt and nitrogen at high reaction temperatures might contribute to the slight deactivation of the catalyst.

3.3. Discussion

In consideration of the results of catalyst characterization and the reactions, we concluded that three factors may contribute to the improvement of the performance of the Pt/NMC catalyst for the decarboxylation of fatty acids. First of all, NMC and MC supports have larger pore size distribution than AC owning to their mesoporous structure (Table 1), which is greatly beneficial to the mass transfer during the decarboxylation reactions and promotes the reaction rates. Particularly, because of the nitrogen doping, the NMC support has the strong electron donor nature of N which could promote enhancement in *p*-bonding, leading to the improvement of electron transfer rate. Besides, the introduction of nitrogen species plays a significant role in anchoring and dispersing Pt particles. It has been confirmed by TEM (Fig. 2) that Pt nanoparticles on NMC exhibit the finest size with the best dispersion among Pt/NMC, Pt/MC and Pt/AC (Table 1). This may result from the enhanced affinity among Pt nanoparticles, which can facilitate nucleation sites to promote a high dispersion of Pt nanoparticles on the surface of the support and finally provide more active sites for the decarboxylation reactions of fatty acids [48,53]. Finally, we believe that the basic sites provided by N species, which was verified by the CO_2-TPD experiment, would be beneficial to adsorbing fatty acids in a more efficient way than those in the N-free MC and AC supports. After decarboxylation reaction, the acid-base interaction between the N species and the formed alkanes no longer exists. As a result, the decarboxylation reaction is improved. Therefore, we consider that mesoporous NMC is a promising alternative support for the decarboxylation of fatty acids. So far, to find a thermal-stable support that can bear such high decarboxylation temperature as more than 300 °C is as urgent as to select an ideal metal. This is the original intention that we designed NMC as the support since carbon materials is quite inert at the reaction temperature in absence of air. Based on the experimental data, we consider that Pt/NMC is a fairly advantageous catalyst for decarboxylation of saturated fatty acids.

In our work, four saturated fatty acids including lauric (C12:0), myristic (C14:0), palmitic (C16:0) and stearic (C18:0) acids with different chain length were used as model substrates for the ultimate goal of decarboxylation reactions. We can see from the initial reaction rates (Table 4) that the influence of the chain length of the substrates on the decarboxylation rate is not very significant. The reaction occurs at the end of carboxylic group of fatty acids and forms alkanes by removal of CO_2. Similar results have also been reported by other research groups [37,69]. However, monounsaturated oleic acid (C18:1) with single carbon–carbon double bond is more easily decarboxylated than polyunsaturated linoleic acid

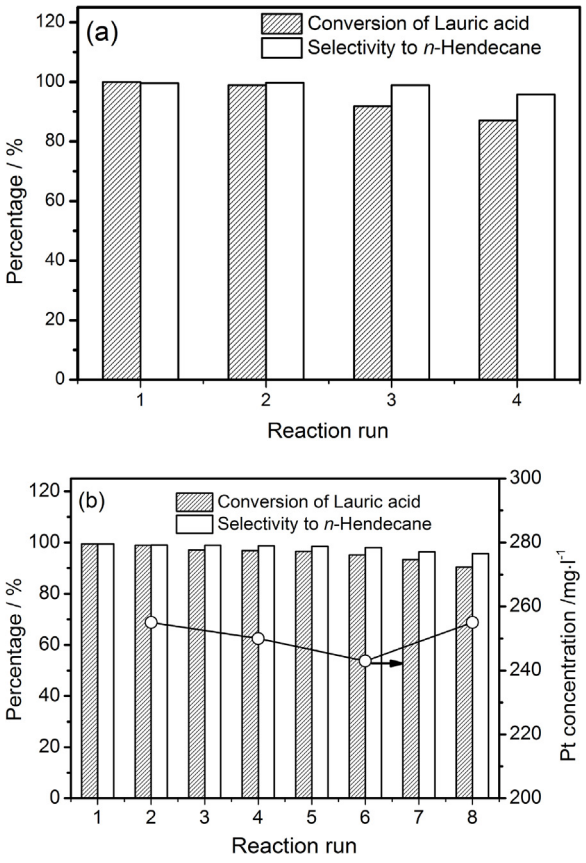

Fig. 7. Recyclability of Pt/NMC catalyst for lauric acid decarboxylation at 15 mg catalyst + 50 mg lauric acid (a) and 50 mg catalyst + 150 mg lauric catalyst (b). Other reaction conditions: T, 330 °C; reaction for 3 h in the same Swagelok mini-reactor.

(C18:2), indicating that the number of C=C bonds in fatty acid molecule affects greatly on the decarboxylation reaction.

Since natural lipid contains fatty acid units with different C=C saturation levels, the research about the effect of saturation level of the fatty acids would be much helpful for the ultimate target in the research field of decarboxylation of natural lipids.

4. Conclusions

Nitrogen-doped mesoporous carbon (NMC) was successfully prepared by a dual-templating approach employing tetraethyl orthosilicate as hard template, Pluronic F127 as soft template and melamine-phenol-formaldehyde resin as both carbon and nitrogen precursors, respectively, and used as the support to prepare Pt nanoparticles catalyst for the decarboxylation of fatty acids. The characterization results revealed that the nitrogen in NMC was in the forms of pyridinic-N (N-6), pyrrolic-N (N-5), graphitic-N (N-Q) and pyridine nitrogen-oxide. The former two forms provided the main initial nucleation sites for the deposition of Pt, and the Pt nanoparticles were more uniformly supported on NMC with average particle sizes of 2.2 ± 1.2 nm, smaller than those on MC and AC (3.1 ± 1.6 nm and 4.7 ± 1.6 nm, respectively). The negative shift of Pt binding energy in Pt/NMC indicates the stronger interaction between N and Pt nanoparticles, which is beneficial to the decarboxylation reactions. Such Pt/NMC catalyst exhibited higher performance than Pt/MC and Pt/AC for the decarboxylation of fatty acids to *n*-alkanes, with the yields of the corresponding alkanes more than 97% for saturated fatty acids and 44.0%-63.6% for unsaturated fatty acids at 330 °C for 3 h. The catalyst could be reused at least seven times with only 9.1% decrease of the yield. The slight deactivation of the catalyst may be ascribed to the aggregation of the Pt particles and the leakage of Pt and nitrogen. The improvement of the catalytic performance of the Pt/NMC catalyst might owe to the introduction of N species to the mesoporous carbon support, which can not only improve the mass transfer during the decarboxylation reactions but also be beneficial to anchoring Pt nanoparticles to form small particle size with better dispersion as well as providing basic sites to adsorb fatty acids to promote the decarboxylation reactions conducting in a more efficient way.

Acknowledgements

This research was supported by the National Natural Science Foundation of China (21476211 and 21276230) and the Zhejiang Provincial Natural Science Foundation of China (LY16B060004).

Appendix A. Supplementary data

Supplementary data associated with this article can be found, in the online version, at http://dx.doi.org/10.1016/j.apcatb.2017.06.065.

References

[1] Z.J. Wei, Y.X. Liu, T. Dilantha, Q.L. Ren, Green Chem. 14 (2012) 1220–1226.
[2] Y.X. Liu, Z.B. Li, Y. Yang, Y.X. Hou, Z.J. Wei, RSC Adv. 4 (2014) 42035–42038.
[3] Z.J. Wei, C.M. Su, D.C. Guo, J.T. Lou, Y.X. Liu, S.G. Deng, ChemSusChem 10 (2017) 1720–1732.
[4] Z.J. Wei, J.T. Lou, Z.B. Li, Y.X. Liu, Catal. Sci. Technol. 6 (2016) 6217–6225.
[5] T.B. Celic, M. Grilc, B. Likozar, N.N. Tusar, ChemSusChem 8 (2015) 1703–1710.
[6] M. Grilc, B. Likozar, J. Levec, ChemCatChem 8 (2016) 180–191.
[7] M. Grilc, B. Likozar, J. Levec, Appl. Catal. B: Environ. 150 (2014) 275–287.
[8] L. Nazari, Z. Yuan, S. Souzanchi, M.B. Ray, C. Xu, Fuel 162 (2015) 74–83.
[9] W.C. Wang, C.J. Bai, Nirajan Thapaliya, Int. J. Energy Res. 39 (2015) 1083–1093.
[10] E. Meller, U. Green, Z. Aizenshtat, Y. Sasson, Fuel 133 (2014) 89–95.
[11] H. Shi, J. Chen, Y. Yang, S. Tian, Fuel Process. Technol. 118 (2014) 161–170.

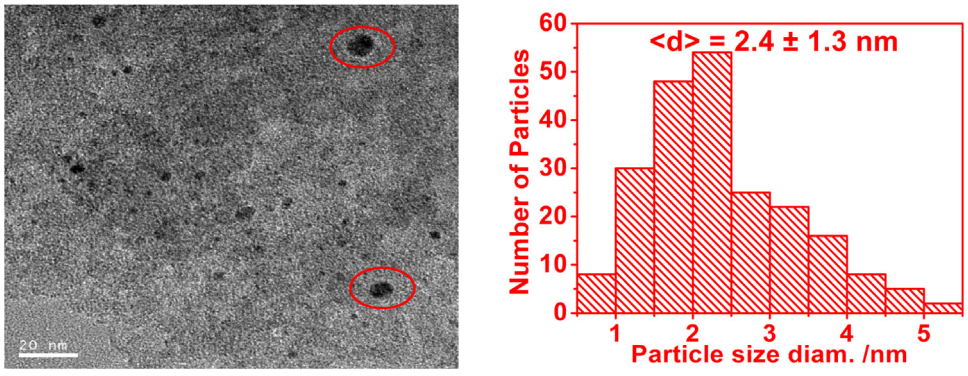

Fig. 8. TEM image of Pt/NMC after eight-cycle used.

[12] E. Santillan-Jimenez, T. Morgan, J. Shoup, A.E. Harman-Ware, M. Crocker, Catal. Today 237 (2014) 136–144.
[13] A.T. Madsen, E.H. Ahmed, C.H. Christensen, R. Fehrmann, A. Riisager, Fuel 90 (2011) 3433–3438.
[14] O.B. Ayodele, H.F. Abbas, W.M.A.W. Daud, Energy Fuels 28 (2014) 5872–5881.
[15] M. Snare, I.K. kova, P. Maki-Arvela, K. Eranen, D.Y. Murzin, Ind. Eng. Chem. Res. 45 (2006) 5708–5715.
[16] J. Fu, X. Lu, P.E. Savage, Energy Environ. Sci. 3 (2010) 311–317.
[17] P.T. Do, M. Chiappero, L.L. Lobban, D.E. Resasco, Catal. Lett. 130 (2009) 9–18.
[18] Y.Y. Chu, J. Cao, Z. Dai, X.Y. Tan, J. Mater. Chem. A 2 (2014) 4038–4044.
[19] T. Wang, C.X. Zhang, X. Sun, Y.X. Guo, H. Guo, J. Tang, H. Xue, M. Liu, X. Zhang, L. Zhu, Q. Xie, J. He, J. Power Sources 212 (2012) 1–12.
[20] S. Lestari, P. Mäki-Arvela, K. Eränen, J. Beltramini, G.Q. Max Lu, D.Y. Murzin, Catal. Lett. 134 (2009) 250–257.
[21] J. Gorka, A. Zawislak, J. Choma, M. Jaroniec, Appl. Surf. Sci. 256 (2010) 5187–5190.
[22] X.J. He, K. Xie, R.C. Li, M.B. Wu, Mater. Lett. 115 (2014) 96–99.
[23] M. Arend, T. Nonnen, W.F. Hoelderich, J. Fischer, J. Groos, Appl. Catal. A: Gen. 399 (2011) 198–204.
[24] X. Ma, G. Ning, Y. Kan, Y. Ma, C. Qi, B. Chen, Y. Li, X. Lan, J. Gao, Electrochim. Acta 150 (2014) 108–113.
[25] J.G. Immer, M.J. Kelly, H.H. Lamb, Appl. Catal. A: Gen. 375 (2010) 134–139.
[26] B. Chang, Y. Li, Y. Guo, H. Yin, S. Zhang, B. Yang, J. Porous Mater. 22 (2015) 629–634.
[27] Gang Wu, De Yu Li, Chang Song Dai, Dian Long Wang, N. Li, Langmuir 24 (2008) 3566–3575.
[28] L. Perini, C. Durante, M. Favaro, V. Perazzolo, S. Agnoli, O. Schneider, G. Granozzi, G. Armando, Appl. Mater. Interfaces 7 (2015) 1170–1179.
[29] Z.B. Lei, L.Z. An, L.Q. Dang, M.Y. Zhao, J.Y. Shi, S.Y. Bai, Y.D. Cao, Microporous Mesoporous Mat. 119 (2009) 30–38.
[30] S.H. Liu, J.R. Wu, Int. J. Hydrogen Energy 36 (2011) 87–93.
[31] E.W. Ping, R. Wallace, J. Pierson, T.F. Fuller, C.W. Jones, Microporous Mesoporous Mat. 132 (2010) 174–180.
[32] Kelly D. Maher, Kathlyn M. Kirkwood, Murray R. Gray, D.C. Bressle, Ind. Eng. Chem. Res. 15 (2008) 5328–5336.
[33] J.G. Na, B.E. Yi, J.K. Han, Y.K. Oh, J.H. Park, T.S. Jung, S.S. Han, H.C. Yoon, J.N. Kim, H. Lee, C.H. Ko, Energy 47 (2012) 25–30.
[34] J.P. Yang, Y.P. Zhai, Y.H. Deng, D. Gu, Q. Li, J. Colloid Interface Sci. 342 (2010) 579–585.
[35] J.Y. Cao, X.J. Yin, L.D. Wang, M.W. Guo, J. Xu, Z.D. Chen, Int. J. Hydrogen Energy 40 (2015) 2971–2978.
[36] Z.J. Wei, Y. Yang, Y.X. Hou, Y.X. Liu, X.D. He, S.G. Deng, ChemCatChem 6 (2014) 2354–2363.
[37] J. Fu, X. Lu, P.E. Savage, ChemSusChem 4 (2011) 481–486.
[38] J. Fu, F. Shi, L.T. Thompson, X. Lu, P.E. Savage, ACS Catal. 1 (2011) 227–231.
[39] Fabing Su, Jianhuang Zeng, Xiaoying Bao, Yaoshan Yu, Jim Yang Lee, X.S. Zhao, Chem. Mater. 17 (2005) 3960–3967.
[40] Y.X. Liu, Y.J. Gu, Y.X. Hou, Y. Yang, S.G. Deng, Z.J. Wei, J. Chem. Eng. 275 (2015) 271–280.
[41] Z.J. Wei, R.F. Pan, Y.X. Hou, Y. Yang, Y.X. Liu, Sci. Rep. 5 (2015) 3089–3092.
[42] J. Yu, M.Y. Guo, F. Muhammad, A.F. Wang, G.L. Yu, H.P. Ma, G.S. Zhu, Microporous Mesoporous Mat. 190 (2014) 117–127.
[43] D. Zhang, L. Zheng, Y. Ma, L. Lei, Q. Li, Y. Li, H. Luo, H. Feng, Y. Hao, ACS Appl. Mater. Interface 6 (2014) 2657–2665.
[44] Y. Lv, F. Zhang, Y. Dou, Y. Zhai, J. Wang, H. Liu, Y. Xia, B. Tu, D. Zhao, J. Mater. Chem. 22 (2012) 93–99.
[45] C. Hsu, J. Jan, H. Lin, P. Kuo, New J. Chem. 38 (2014) 5521–5526.
[46] J. Zhang, L. Ma, M. Gan, F. Yang, S. Fu, X. Li, J. Power Sources 288 (2015) 42–52.
[47] B. Yue, Y. Ma, H. Tao, L. Yu, G. Jian, X. Wang, X. Wang, Y. Lu, Z. Hu, J. Mater. Chem. 18 (2008) 1747–1750.
[48] L. Zhang, Z. Wang, J. Zhang, X. Sui, L. Zhao, D. Gu, Carbon 93 (2015) 1050–1058.
[49] C. Li, V. Malgras, S.M. Alshehri, J.H. Kim, Y. Yamauchi, Electrochim. Acta 183 (2015) 107–111.
[50] F. Fina, H. Ménard, J.T.S. Irvine, Phys. Chem. Chem. Phys. 17 (2015) 13929–13936.
[51] D.S. Park, D. Yun, T.Y. Kim, J. Baek, Y.S. Yun, J. Yi, ChemSusChem 6 (2013) 2281–2289.
[52] H. Huang, Q. Wang, Q. Wei, Y. Huang, Int. J. Hydrogen Energy 40 (2015) 6072–6084.
[53] S.H. Liu, M.T. Wu, Y.H. Lai, C.C. Chiang, N. Yu, S.B. Liu, J. Mater. Chem. 21 (2011) 12489–12496.
[54] M. Chen, L. Shao, Y. Liu, T. Ren, Z. Yuan, J. Power Sources 283 (2015) 305–313.
[55] Y. Song, L. Li, Y. Wang, C. Wang, Z. Guo, Y. Xia, ChemPhysChem 15 (2014) 2084–2093.
[56] J. Choma, K. Jedynak, W. Fahrenholz, J. Ludwinowicz, M. Jaroniec, Appl. Surf. Sci. 289 (2014) 592–600.
[57] Z.S. Li, D.H. Li, Z.H. Liu, B.L. Li, C.Y. Ge, Y.P. Fang, Electrochim. Acta 158 (2015) 237–245.
[58] D. Saha, S.G. Deng, Langmuir 25 (2009) 12550–12560.
[59] Jing Xuan Cai, Simona Bennici, J.Y. Shen, A. Auroux, React. Kinet. Mech. Catal. 115 (2015) 263–282.
[60] X.X. Liu, H. Zhu, X.R. Yang, J. Power Sources 262 (2014) 414–420.
[61] K.Y. Chun, H.S. Lee, C.J. Lee, Carbon 47 (2009) 169–177.
[62] S. Gao, H. Fan, X. Wei, L. Li, Y. Bando, D. Golberg, Part. Part. System Charact. 30 (2013) 864–872.
[63] S.C. Roya, A.W. Hardinga, A.E. Russellb, K.M. Thomas, J. Electrochem. Soc. 144 (1997) 2323–2328.
[64] F.F. Wang, S. Shao, C.L. Liu, C.L. Xu, R.Z. Yang, W.S. Dong, J. Chem. Eng. 264 (2015) 336–343.
[65] G. Abdulkareem-Alsultan, N. Asikin-Mijan, H.V. Lee, Y.H. Taufiq-Yap, J. Chem. Eng. 304 (2016) 61–71.
[66] J. Xu, T. Chen, Q. Jiang, Y.X. Li, J. Chem. Asian 9 (2014) 3269–3277.
[67] C. Goel, H. Bhunia, P.K. Bajpai, J. Environ. Sci. (China) 32 (2015) 238–248.
[68] J. Yu, M.Y. Guo, F. Muhammad, A.F. Wang, F. Zhang, Q. Li, G.S. Zhu, Carbon 69 (2014) 502–514.
[69] I. Simakova, O. Simakova, P. Mäki-Arvela, D.Y. Murzin, Catal. Today 150 (2010) 28–31.